Earth Planets Space, **65**, 893–900, 2013

Caldera structure of submarine Volcano #1 on the Tonga Arc at 21°09′S, southwestern Pacific: Analysis of multichannel seismic profiling

Han-Joon Kim[1], Hyeong-Tae Jou[1], Gwang-Hoon Lee[2], Ji-Hoon Na[3], Hyun-Sub Kim[1], Ugeun Jang[4], Kyeong-Yong Lee[1], Chang-Hwan Kim[1], Sang Hoon Lee[1], Chan-Hong Park[1], Seom-Kyu Jung[1], and Bong-Cool Suk[1]

[1]*Korea Institute of Ocean Science and Technology, Ansan 426-744, Korea*
[2]*Department of Energy Resources Engineering, Pukyong National University, Korea*
[3]*POSCO Technical Research Laboratories, Pohang, Korea*
[4]*School of Earth and Environment, University of Western Australia, Perth, Australia*

(Received September 3, 2012; Revised December 13, 2012; Accepted January 7, 2013; Online published September 17, 2013)

Volcano #1 is a large submarine stratovolcano with a summit caldera in the south central part of the Tonga Arc. We collected and analyzed multichannel seismic profiles in conjunction with magnetic data from Volcano #1 to investigate the structure of the intracaldera fill and processes of caldera formation. The intracaldera fill, exhibiting stratified units with a maximum thickness of 2 km, consists of at least four seismic units and a thick wedge of landslide debris derived from the caldera wall. The structural caldera floor, deepening toward the northwestern rim, suggests asymmetric collapse in the initial stage, which, in turn, appears to have contributed to the creation of a caldera elongated to the northwest by enhancing gravitational instability along the northwestern caldera boundary. Occasional, but repeated, eruptions resulted in a thick accumulation of the intracaldera fill and further subsidence in the mode of piston collapse. Magnetization lows are well-defined along the structural rim of the caldera that is interpreted as the inner principal ring fault. The magnetization lows indicate sites of submarine hydrothermal vents that caused an alteration of magnetic minerals. Faults recognized on the outer slope of the volcano are interpreted to be involved in hydrothermal fluid circulation.

Key words: Tonga Arc, Volcano #1, multichannel seismic sections, caldera infill, seismic unit, magnetic anomaly, hydrothermal activity.

1. Introduction

The Tonga-Kermadec Arc-backarc system in the southwestern Pacific is one of the most volcanically and seismically active subduction zones on Earth (Arculus, 2005). The Tonga-Kermadec intra-oceanic Arc is part of the Tonga-Kermadec Arc-backarc system (Fig. 1). The Tonga-Kermadec Arc is divided into two main parts: the Tonga Arc in the north (from 16°S to 27°S, ∼1300 km long) and the Kermadec Arc in the south (from 27°S to 38°S, ∼1200 km long) (Schwarz-Schampera *et al*., 2007). Recent discoveries by multibeam swath bathymetry, hydrothermal plume mapping, and rock dredging, have documented topography, petrology, and hydrothermal venting, of the volcanic edifices on the Tonga-Kermadec Arc (Arculus, 2005). The volcanic edifices comprise stratovolcanoes of variable complexity and steep-walled calderas with diameters <12 km. About 40 percent of these are hydrothermally active (Arculus, 2005) and therefore hydrothermal venting in the Tonga-Kermadec Arc has become a widely recognized process. Sites of hydrothermal venting are commonly located at summit or intracaldera cones, and also near the base of the caldera walls (Arculus, 2005). The depth range of hydrothermal plumes along the Kermadec Arc varies from 180 to 1800 m, implying that the arc represents a potentially extensive source of shallow vent fields expelling fluids into the Pacific (de Ronde *et al*., 2001).

Of the volcanoes on the Tonga Arc, Volcano #1 in the south central part of the Tonga Arc has been explored repeatedly by submersible dives (Stoffers *et al*., 2006; Schwarz-Schampera *et al*., 2007; Hekinian *et al*., 2008). Volcano #1, constructed recently by explosive volcanism alternating with quieter explosive events, is characterized by a well-defined caldera structure on the summit and active hydrothermal venting in a widespread diffuse manner (Stoffers *et al*., 2006; Hekinian *et al*., 2008).

Intracaldera fill provides evidence of caldera formation processes. Many large calderas collapse during eruptions that emplace ash-flow tuffs within the subsided area, and, later, caldera-wall slide breccias concentrate along caldera margin walls (Lipman, 1997). Little is known about the structure of the intracaldera fill in Volcano #1 and the processes of caldera formation associated with its subsidence. In this study, we collected and analyzed multichannel seismic (MCS) and magnetic data from Volcano #1 to investigate the structure and emplacement of the caldera infill associated with subsidence.

2. Morphology Volcano #1 and Hydrothermal Activity

Volcano #1 is a large stratovolcano with a basal diameter of ∼28 km located at the rear of the south central part

Copyright © The Society of Geomagnetism and Earth, Planetary and Space Sciences (SGEPSS); The Seismological Society of Japan; The Volcanological Society of Japan; The Geodetic Society of Japan; The Japanese Society for Planetary Sciences; TERRAPUB.

doi:10.5047/eps.2013.01.002

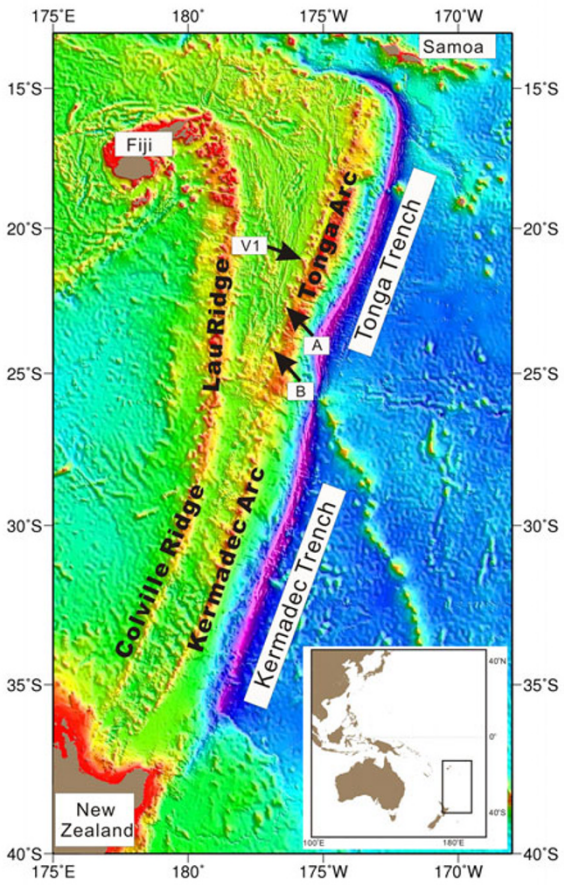

Fig. 1. Location map showing the Tonga Arc, the Kermadec Arc, the Tonga Trench, and the Kermadec Trench. V1 is Volcano #1 on the Tonga Arc. A and B are volcanoes with a summit caldera located adjacent to Volcano #1 (see Fig. 7 for bathymetry). The area is indicated by a rectangle in the inset.

of the Tonga Arc (Fig. 1), rising from the flat seafloor at ~1800 mbsl (meters below sea level) to a summit at 65 mbsl (Fig. 2(a)). Volcano #1 was recently built by successive and numerous short-lived volcanic eruptions of pyroclastic deposits alternating with quieter, intermittent outpouring of massive lava flows (Hekinian *et al.*, 2008).

A large caldera, defined by a relatively-well-preserved rim, occurs on the summit (Schwarz-Schampera *et al.*, 2007) (Fig. 2). The caldera, measuring 7 km × 4.5 km, is elliptic or oval-shaped, elongated northwest-southeast. The elongation direction of the caldera is subparallel to the north-northwest direction of subduction of the Pacific Plate at the Tonga Trench and the compression axis of shallow thrust-type earthquakes in the Tonga Arc (Pelletier *et al.*, 1998). Most of the caldera rim ranges between 150 and 400 mbsl, with the highest areas on the southeastern rim and the lowest to the southwest. The center of the caldera is embossed with a large east-sloping plateau bounded by a circular ridge 2.8 km in diameter that ranges from <50 m above the caldera floor in the east to 250 m above the caldera floor in the west (Schwarz-Schampera *et al.*, 2007). This ridge-bounded plateau was termed the V1P1 cone by Schwarz-Schampera *et al.* (2007). Two smaller post-caldera cones are present between the western margin of the V1P1 cone and the western caldera rim: one to the northwest and the other to the southwest each termed V1P2 and V1P3, respectively (Schwarz-Schampera *et al.*, 2007). The V1P2 cone has a diameter of 1.3 km with a summit depth of 150 m, and rises 300 m above the caldera floor. The V1P3 cone has a diameter of 1.2 km with a summit depth of 90 m, and rises 350 m above the caldera floor. The cones of V1P1, V1P2, and V1P3 were constructed by occasional eruptions of coarse pyroclast-ash flow after the major caldera collapsed (Hekinian *et al.*, 2008). Hydrothermal activity at

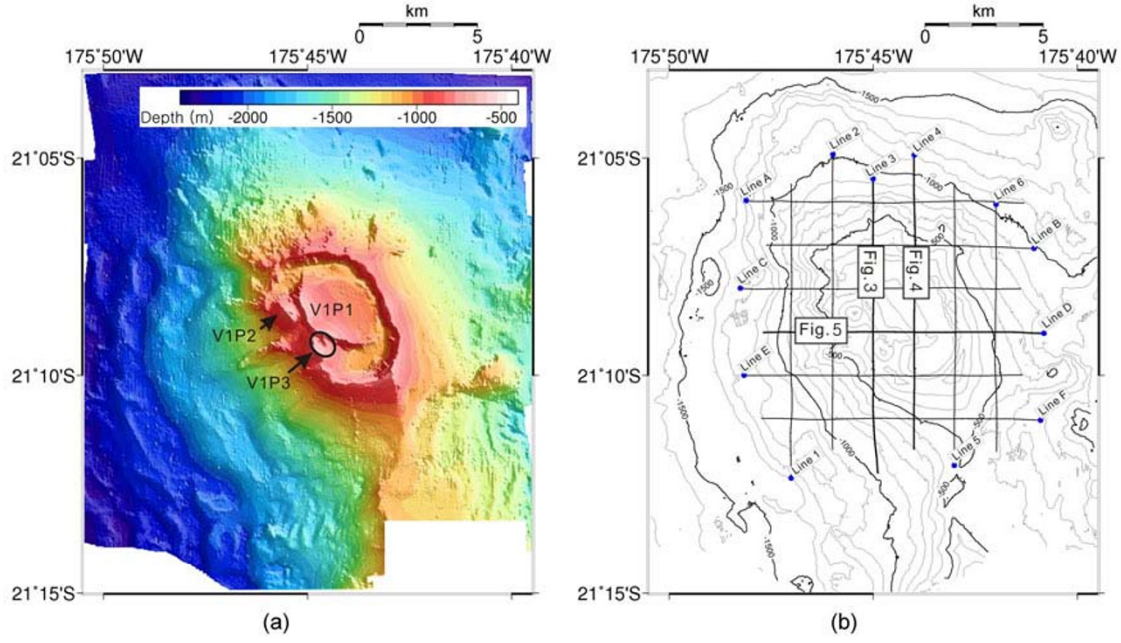

Fig. 2. (a) Bathymetry of Volcano #1. (b) Locations of MCS seismic profiles. The locations of the seismic profiles shown in this study are plotted as thick lines labeled with a figure number. A chain of craters is denoted by a circle.

Volcano #1 was observed in many places in the caldera including the flank of the V1P3 cone. On the flank of the V1P3 cone, a chain of three explosion craters, each less than 500 m wide and as deep as 100 m, occurs (Fig. 2(a)). Widespread diffuse hydrothermal venting, vigorous gas discharge, and thick beds of sulfur-cemented ash were reported at water depths of 160–210 m in and around the crater chain (Stoffers *et al*., 2006). Here, massive native sulfur and strongly altered volcaniclastic rocks are present (Schwarz-Schampera *et al*., 2007). In addition to this, Dive Pisces IV-143 discovered evidence of hydrothermal activity in the caldera floor immediately inward of the northeastern caldera wall, where greenish yellow powder-like material was observed covering black ash (Hekinian *et al*., 2008).

3. Data Acquisition and Processing

The MCS and magnetic data were acquired on the R/V Onnuri of the Korea Institute of Ocean Science and Technology (KIOST) in 2008. The MCS survey grid consists of six north-south and six east-west lines spaced at 1-minute intervals each 12 km long on average (Fig. 2(b)). Shots from an eight air gun, 690 in^3 source array were recorded on a 108 channel streamer. Shot spacing and channel interval were 12.5 m, providing 54-fold coverage. The MCS data were processed using Geovecteur Plus®. The processing sequence followed standard procedures including velocity analysis, stack, multiple suppression after stack using predictive deconvolution, time-varying band-pass filtering, finite-difference time migration, and time-to-depth conversion using the interval velocity information.

Magnetic data were obtained along the MCS survey lines using a surface-towed magnetometer. The total magnetic field was recorded using a proton magnetometer system sampling at 1-second intervals. Diurnal variations in the magnetic field were not recorded locally during the survey. The data were corrected for secular variation by subtracting a regional magnetic field based on IGRF (International Geomagnetic Reference Field) 2005. The corrected data were inverted for crustal magnetization by the method of Parker and Huestis (1974) assuming a constant source layer of 300 m.

4. Results

4.1 Structure of the caldera on Volcano #1

A volcano with a caldera at the summit consists of various morphologic elements including: topographic rim, inner caldera wall, caldera-bounding faults, structural caldera floor, and intracaldera fill (mainly landslide debris from caldera walls and ponded ash-flow tuff) (e.g. Lipman, 1997). The depth-converted MCS profiles demonstrate the overall structure of the caldera and intracaldera fill of Volcano #1 (Figs. 3 to 5). The topographic rim is depicted on the MCS profiles as a pointed escarpment that bounds the subsided area. At the southwestern flank, the topographic rim is buried by erupted material (Fig. 5). The V1P1 cone is composed of layered deposits; however, seismic reflection signals are highly disrupted below the V1P3 cone, making it difficult to recognize layering.

On the basis of external and internal seismic facies, four key seismic units that constitute the V1P1 cone were recognized as the caldera infill. They are seismic sequences bounded by reflecting horizons that are consistently traced in seismic profiles. These seismic units are referred to as U-1 to U-4 from oldest to youngest. Hekinian *et al*. (2008) suggested that post-caldera cones were constructed by occasional eruptions dominantly of coarse pyroclast-ash flow. Therefore, we interpret that seismic units of U-1 to U-4 consist dominantly of these materials. No age can be assigned to the seismic units. Hekinian *et al*. (2008) identified about 20 volcaniclastic units along the caldera wall and suggested a short-time interval of about decades between eruptions, based on the presence of fresh scoria and fresh lava flows and the absence of non-volcanic sediments within volcanic deposits. Therefore, they estimated the overall caldera wall to have been constructed probably during the last 200 years. The seismic units are likely to be younger than the caldera wall because they constitute the post-caldera cone of V1P1. Landslide debris is created by sliding and slumping triggered by gravitational instability during and after caldera collapse. Consequently, landslide debris tends to accumulate as debris fans adjacent to margins of the subsided block (Lipman, 1997) that would appear as a wedge thickening downwards on seismic profiles. The reflectors dipping inward below the structural rim are interpreted to be oblique sides of the landslide debris wedges (Figs. 3–5). The base of the caldera fill corresponding to the acoustic basement is not clearly distinguished. Instead, it is only locally identifiable under the V1P1 cone in the center of the caldera due to limited penetration. It is not imaged adjacent to the caldera rim where a thick accumulation of landslide debris occurs. The visible acoustic basement dips down toward the northwestern caldera rim.

Although the MCS profiles enable us to recognize the layering of the caldera infill, the caldera-bounding faults are not properly imaged, which we ascribe to the following reasons. First, the caldera-bounding faults, in most cases, are very steeply dipping or near-vertical (Cole *et al*., 2005). Surface seismic data do not contain energy reflected from those faults regardless of acquisition geometry. As the second explanation, the landslide debris, stacked chaotically down the caldera-bounding fault plane, scatters seismic waves. In addition, the caldera boundary consists of laterally-varying or discontinuous elements such as topographic rim, inner caldera wall, caldera-bounding faults, and slided/slumped material from the wall. Diffractions and multiple reflections from these morphologically complicated elements are difficult to remove completely and mask internal structure. We estimated the locations of the caldera-bounding faults by correlating the MCS profiles with the magnetic anomaly profiles (discussed later in Section 4.2).

U-1 is the deepest unit underneath the V1P1 cone. The detailed internal layering of U-1 is difficult to interpret due to deep burial and deterioration of data quality. It is thick in the northwestern part of the caldera and thins southeastward. The seismic facies of U-1 is characterized by multiple layers of short, complex, and irregular, high-amplitude reflections with poor continuity. The high-amplitude reflections are suggestive of highly-reflective volcanic lava sill/flow. It thus appears that U-1 consists of volcanic ash

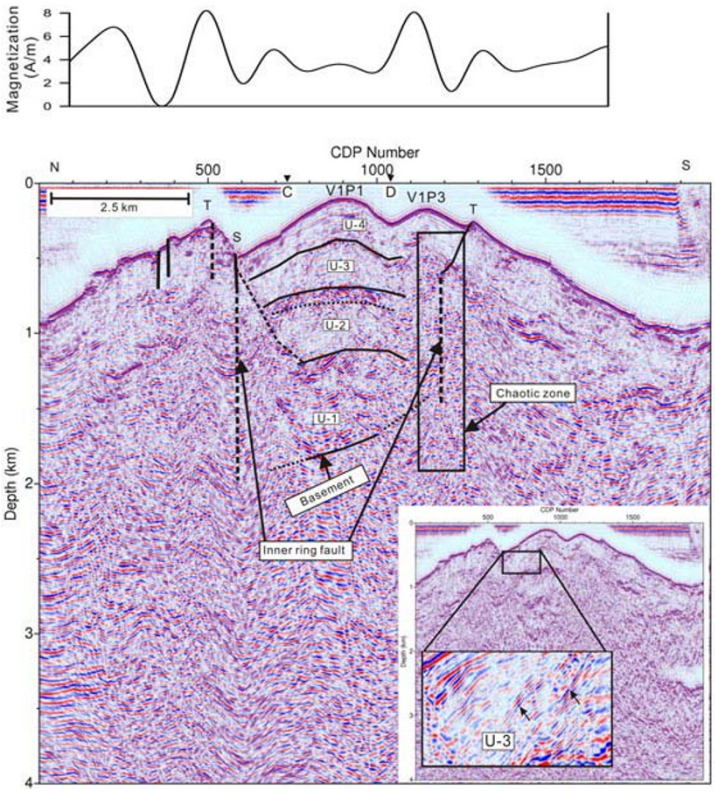

Fig. 3. MCS section of Line 03 with interpretive line drawings (see Fig. 2(b) for location). Triangles indicate the intersecting locations of crossing profiles of C and D. Magnetization profile in the same horizontal scale is also shown in the above. D = subsidence depth, T = topographic rim, and S = structural rim. Caldera-bounding faults, which typically dip steeply (e.g., Lipman, 1997), are arbitrarily shown as vertical (dashed lines). The inset shows the uninterpreted section. The close-up in the inset highlights toplap configuration in U-3 indicated by arrows.

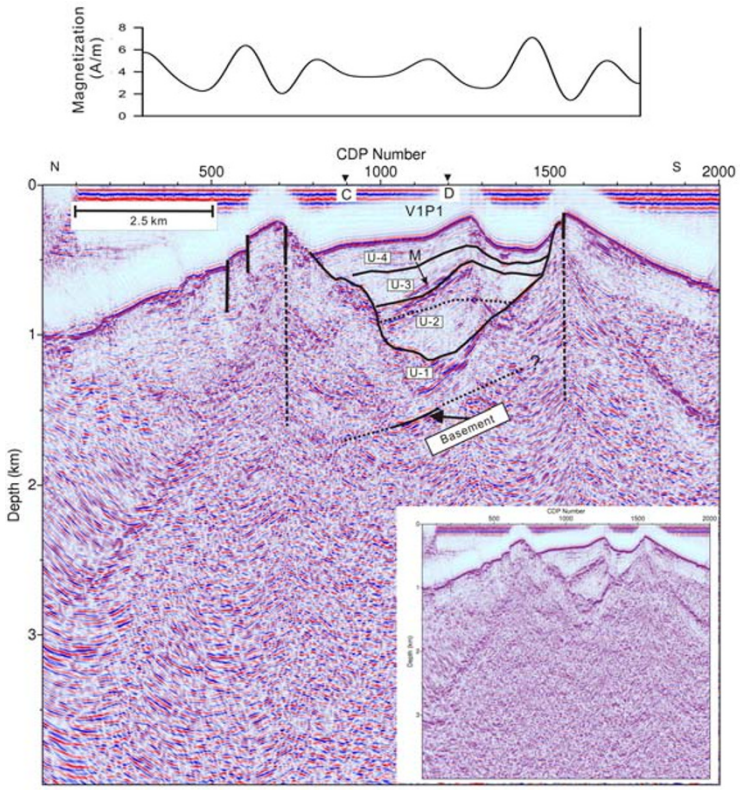

Fig. 4. MCS section of Line 04 with interpretive line drawings (see Fig. 2(b) for location). M denotes the multiple reflection of the seafloor. Triangles indicate the intersecting locations of crossing profiles of C and D. Magnetization profile in the same scale is also shown in the above. The inset shows the uninterpreted section.

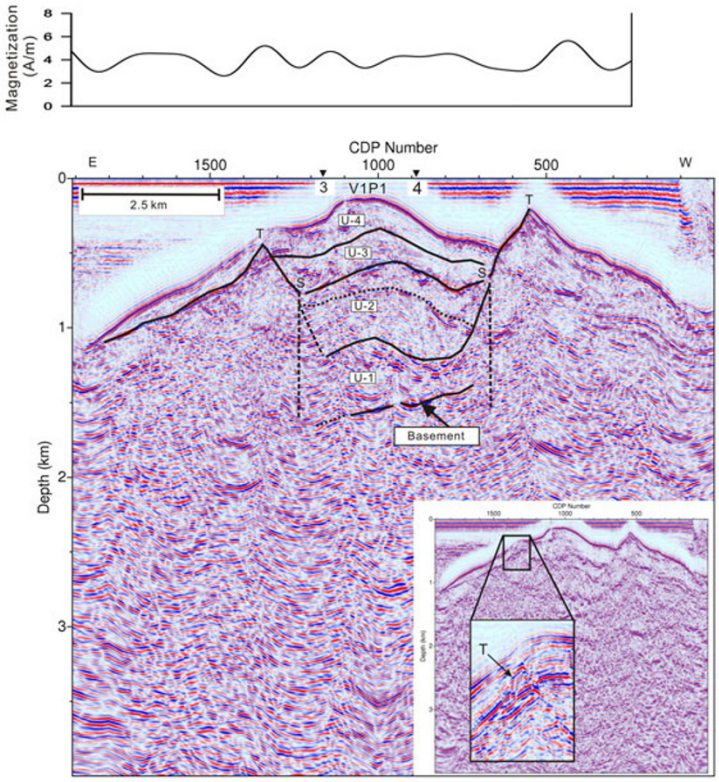

Fig. 5. MCS section of Line D with interpretive line drawings (see Fig. 2(b) for location). Triangles indicate the intersecting locations of crossing profiles of 3 and 4. Magnetization profile in the same horizontal scale is also shown in the above. The inset shows the uninterpreted section. The close-up in the inset highlights the buried topographic rim. T = topographic rim and S = structural rim.

and pyroclastic sediments interbedded with volcanic and lava sill/flow. Because U-1 merges with landslide debris toward the caldera wall, we interpret that U-1 was deposited concurrently with slide debris. The interval velocity of U-1, ranging from 2.9 to 3.1 km/s, indicates significant welding and consolidation of volcaniclastics. The chaotic internal seismic facies of slide debris indicates massive and quick deposition.

U-2 and U-3 consist of low-to-high or variable amplitude, moderate-to-poor continuity reflections that have in places a wave-like character suggestive of deposition by flow processes. These units are accumulated in the entire caldera area. However, they exhibit variations in thickness. U-2 is subdivided into upper and lower layers. Overall, U-2 and U-3 form mounds on the sections, marking the location of the thickest accumulation. When an eruption occurs underwater, the ballistic dispersal of clastic materials is initially very restricted because of the enclosing water (Milia *et al.*, 2000). Additionally, the increasing hydrostatic pressure of the water column with increasing water depth in subaqueous environments limits the ability of superheated volatiles to expand instantaneously against the ambient pressure (Cas, 1992). Thus, the post-caldera eruptive center is likely to be the site of greater thickness of a volcanic sedimentary sequence than elsewhere in the submarine caldera. The internal reflections of U-2 and U-3 display, in places, toplap truncation against the upper surface and downlap onto the underlying surface (Fig. 3), indicating that erupted material was deposited in a prograding manner away from the source.

U-4 is the uppermost unit of the V1P1 cone. The thickness of U-4, ranging from 200 to 300 m in the caldera area, does not vary significantly. This unit consists of a well-stratified succession characterized by good continuity, although a few strong amplitude reflections with poor continuity are visible. The upper part of U-4 mostly comprises weak amplitude (i.e., lack of reflectivity) reflectors that are parallel to the seafloor. The interval velocity of U-4 is around 1.5 km/s. The low amplitude and interval velocity suggest that U-4 consists of relatively homogeneous and unconsolidated volcanic ash and flows that are diffusely bedded. The nearly transparent internal seismic facies may be a result of rapid emplacement. U-4 buries the caldera wall to the west and reaches the lower part of the outer slope of Volcano #1 (Fig. 5).

The V1P3 cone is characterized by chaotic seismic facies that completely masks internal structure (Fig. 3). The uppermost part of the V1P3 cone shows weak layering with subdued internal reflections. Therefore, we anticipate that the V1P3 cone resulted from very rapid deposition of coarse pyroclastic material and ash. The chaotic seismic facies and lack of internal reflections indicate that the V1P3 cone was built by less than a few occasional highly-explosive eruptions.

4.2 Evolution of the caldera and hydrothermal alteration

Experimental studies, observations, and geophysical analysis (Cole *et al.*, 2005; Acocella, 2007, and references therein) suggest that caldera collapse occurs on the steeply outward dipping reverse fault; a second set of outer normal

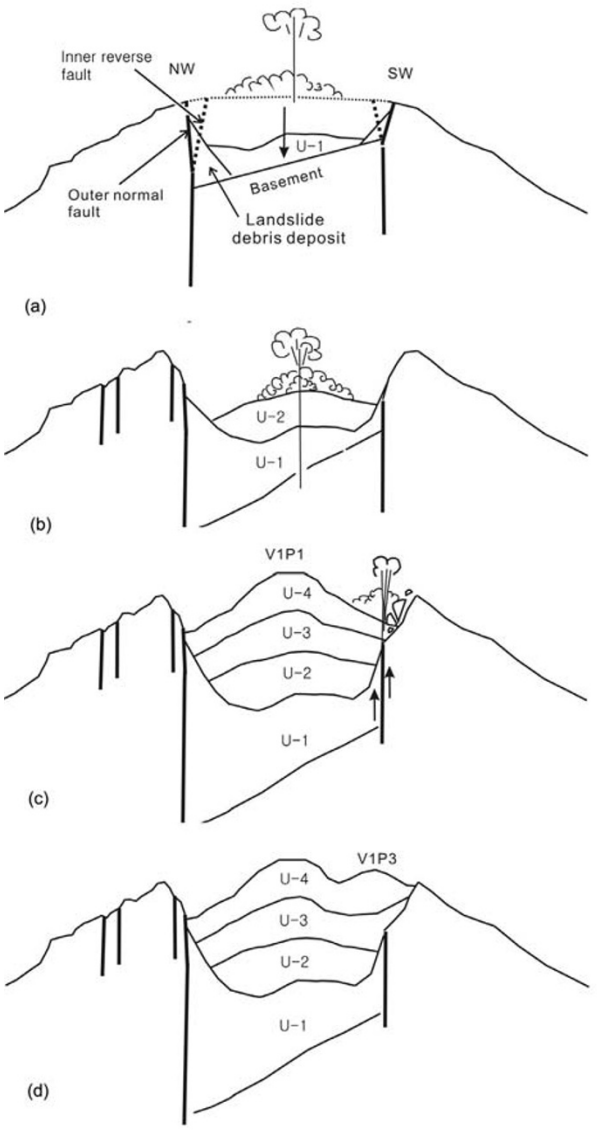

Fig. 6. Schematic diagram showing a possible sequence of events associated with the formation of the caldera in Volcano #1. (a) Initiation of asymmetric collapse. (b) Repeated eruptions and further subsidence. (c) Buildup of the V1P1 cone and neovolcanic eruption along the southwestern rim. (d) Present geologic structure pertaining to Fig. 3.

faults dipping inward, associated with late-stage peripheral extension, develops at the caldera margin. Figure 6 is a conceptual model showing the evolution processes of the Volcano #1 caldera from the initiation of collapse to the present that eventually pertains to the geologic structure shown in Fig. 3. The basement floor deepening flatly toward the northwestern rim creates an asymmetric subsidence structure, which suggests that the collapse initiated in a trapdoor fashion (Fig. 6(a)) with a hinge on the opposite southeastern caldera rim. Asymmetric collapse is a common style of subsidence, either as a trapdoor along a single hinge fault or as a series of blocks (Stix *et al*., 2003). The zone between these inner reverse and outer normal faults became subjected to tilting and fracturing that facilitated landslides. We envisage, therefore, that the Volcano #1 caldera collapsed along the steeply-dipping reverse fault; afterwards, the overhang reverse fault scarp decayed rapidly, emplacing the thick wedge-shaped landslide debris inward of the fault plane.

While the caldera collapsed, it was filled rapidly with erupted material, volcanic sill/flow, and landslide debris deposits (Fig. 6(b)). The shape of a caldera is affected by a regional tectonic control, pre-existing structures, and the depth to which the magma body has intruded (Kusumoto and Takemura, 2005; Acocella, 2007). Volcano #1, like its caldera, is elongated to the northwest. The calderas of other volcanoes adjacent to Volcano #1 on the Tonga Arc are circular or differ from Volcano #1 in elongation direction, sensu stricto (Fig. 7). This observation may indicate that tectonic control here did not play a primary role in shaping the caldera. We further anticipate that the most deeply-subsided zone along the inner reverse fault in the northwestern part of the Volcano #1 caldera created the largest overhang which, in turn, induced enhanced gravitational instability. In this case, the caldera wall probably retreated outward more extensively to the northwest from the rim of the initial collapse as a result of sliding and slumping, facilitating the creation of the caldera elongated to the northwest. While eruptions recurred, the subsiding caldera was successively filled with erupted sequences (Fig. 6(c)) to form the V1P1 cone. Seismic sections indicate that the internal structure of the caldera infill and sequence boundaries experienced little deformation. This feature suggests further subsidence of a coherent block of rock into an evacuating magma chamber along a ring fault that induced piston/plate collapse as eruptions progressed. The undeformed unit boundaries also suggest that subsidence by sediment loading has not occurred noticeably after deposition. The experiment by Kennedy *et al*. (2004) indicates that highly-asymmetrical subsidence is a result of tilting of the magma chamber and the deepest point of an elongate trapdoor caldera occurs where the magma chamber is deepest. Roche *et al*. (2000) suggests from their experiments that shallow magma chambers with large diameters lead to coherent single-block collapse structures, while deep chambers with small diameters lead to a series of multiple nested blocks. It is possible that the collapse of Volcano #1 was associated with a shallow tilted magma chamber. While repeated eruptions occurred, a steeply-dipping fault was created in the hinged segment to complete the caldera-bounding ring-fault system to induce coherent subsidence of the caldera area. After the V1P1 cone had formed, eruptions took place along the arcuate segments of caldera margins to form a smaller cone of V1P3 (Fig. 6(d)).

Calderas are commonly the sites of geothermal activity and mineralization (Cole *et al*., 2005). The principal caldera fault system consisting of inner reverse and outer normal faults is the prime locus of hydrothermal fluid circulation between the surface and the magma chamber underneath, whereby cold sea water is drawn down the normal faults and returns as metal-rich hot fluid along the reverse faults, favoring the formation of volcanogenic massive sulfide (VMS) deposits at caldera wall margins (Mueller *et al*., 2009). A comparison of magnetization values and geologic structure seems to indicate a primary association between them (Figs. 3–5). Magnetization ranges from 0 to 8 A/m. Noticeably, well-defined magnetization lows oc-

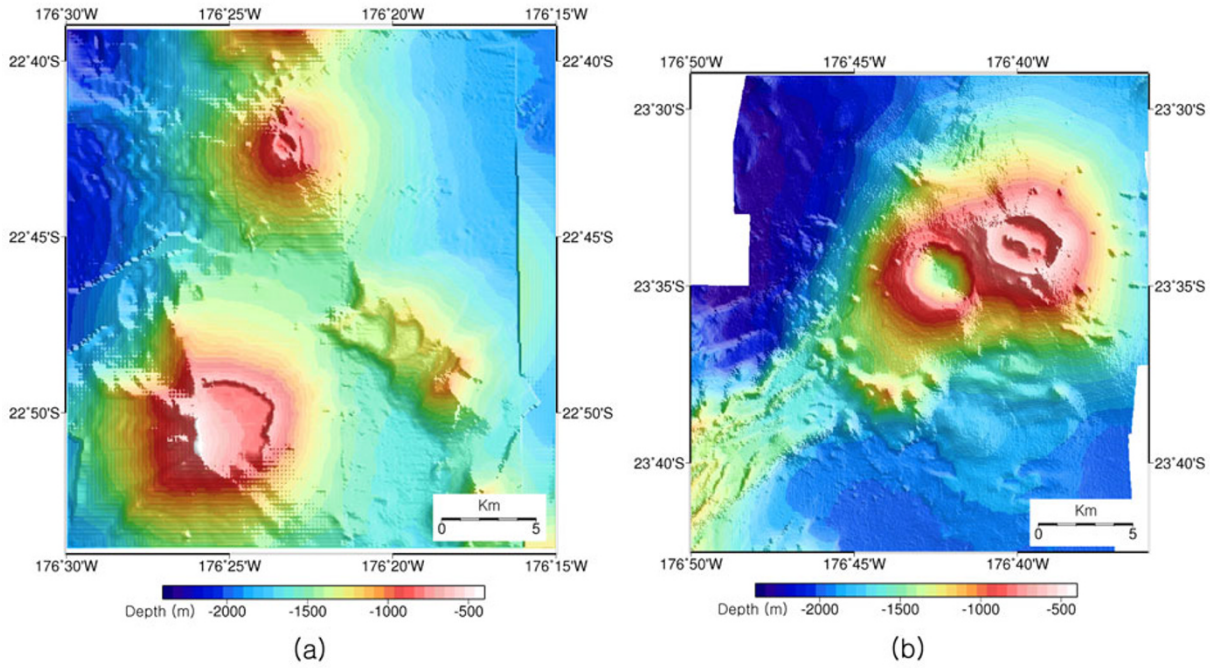

Fig. 7. Bathymetry of volcanoes (a) A, and (b) B, with a summit caldera adjacent to Volcano #1 (see Fig. 1 for location).

cur along the structural rim which represents the inner ring fault. Magnetization lows are likely to be present along the entire structural rim and mark the collapse boundary. Emplacement of sulfide in the Volcano #1 caldera has been reported from submersible dives (e.g., Stoffers *et al*., 2006). Hydrothermal alteration of footwall rocks beneath massive sulfide deposits may lead to the destruction of magnetic phases and results in anomalously low magnetic signals (Morgan, 2012). Magnetization lows above the rim of Volcano #1, therefore, is interpreted to indicate hydrothermal activity along the principal ring fault. Magnetic lows are not observed in the center of the caldera, suggesting that the zone of hydrothermal activity is limitedly present close to the inner ring fault. Topographic displacements that appear to be the surface expressions of steeply-dipping faults are recognized on the outer slope of the volcano as well as on the inner structural rim. The coincidence of their locations with magnetization lows (Figs. 3 to 5) suggests that they constitute the outer ring fault system and are involved in hydrothermal fluid circulation that enables VMS deposits to develop.

The subsidence depth is estimated from seismic profiles by measuring the vertical distance from the top of the topographic rim to the acoustic basement. The maximally recognized depth of the acoustic basement is 2 km inward of the northwestern rim (Fig. 3). The acoustic basement may get deeper toward the caldera rim that marks the site of the principal ring fault. The ratio of the diameter (4.5∼7 km) to subsidence (2 km) of the caldera ranges from 2.3 to 3.5 allowing it to be quantified as a stage 4 caldera according to Acocella (2007). A stage 4 caldera is usually associated with the largest erupted volumes, enabling the emplacement of thick accumulation of the caldera fill as observed on seismic profiles.

5. Conclusions

Multichannel seismic reflection profiles collected in this study reveal the intracaldera fill structure of Volcano #1 in the south central part of the Tonga Arc. The intracaldera fill consists of at least four syneruptive seismic units produced by multi-stage post-caldera eruptions and thick, wedge-shaped landslide debris. The intracaldera fill is thickest (∼2 km) along the northwestern boundary of the caldera. The interval velocity within the intracaldera fill shows a relatively rapid increase with depth from 1.5 km/s in the top unit to about 3 km/s in the bottom unit, which seems to indicate consolidation to a considerable degree. The basement floor is relatively flat but deepens toward the northwestern rim, demonstrating asymmetric subsidence structure. We interpret that collapse initiated in a trapdoor mode with a hinge on the southeastern caldera rim. Further subsidence of the entire structural caldera floor occurred in the mode of piston collapse during occasional, but repeated, eruptions. The caldera wall retreatment was achieved preferentially toward the northwest where gravitational instability was enhanced. Magnetization lows occurring along the structural rim outline the area of collapse guided by the principal ring fault. The magnetization lows are inferred to represent the sites of hydrothermal alteration of magnetic minerals caused by submarine hydrothermal fluid circulation.

Acknowledgments. This work was funded by the Ministry of Oceans and Fisheries of Korea (Grant PM56572) and the Center for Atmospheric Sciences and Earthquake Research (Grant CATER 2012-8100). We thank two reviewers for their insightful review and constructive comments.

References

Acocella, V., Understanding caldera structure and development: An overview of analogue models compared to natural calderas, *Earth Sci. Rev.*, **85**, 125–160, 2007.

Arculus, R. J., Arc-backarc systems of northern Kermadec-Tonga, *Proc. 2005 New Zealand Minerals Conference*, 45–50, 2005.

Cas, R. A. F., Submarine volcanism; eruption styles, products, and relevance to understanding the host-rock successions to volcanic-hosted massive sulfide deposits, *Econ. Geol.*, **87**, 511–541, 1992.

Cole, J. W., D. M. Milner, and K. D. Spinks, Caldera and caldera structures: A review, *Earth Sci. Rev.*, **69**, 1–26, 2005.

de Ronde, C. E. J., E. T. Baker, G. J. Massoth, J. E. Lupton, I. C. Wright, R. A. Feely, and R. R. Greene, Intra-oceanic subduction-related hydrothermal venting, Kermadec volcanic arc, New Zealand, *Earth Planet. Sci. Lett.*, **193**, 359–369, 2001.

Hekinian, R., R. Mühe, T. J. Worthington, and P. Stoffers, Geology of a submarine volcanic caldera in the Tonga Arc: Dive results, *J. Volcanol. Geotherm. Res.*, **176**, 571–582, 2008.

Kennedy, B., J. Stix, J. W. Vallance, Y. Lavallee, and M. A. Longpre, Controls on caldera structure: Results from analogue sandbox modeling, *GSA Bull.*, **116**, 515–524, 2004.

Kusumoto, S. and K. Takemura, Caldera geometry determined by the depth of the magma chamber, *Earth Planets Space*, **57**, e17–e20, 2005.

Lipman, P. W., Subsidence of ash-flow calderas: relation to caldera size and magma-chamber geometry, *Bull. Volcanol.*, **59**, 198–218, 1997.

Milia, A., M. M. Torrente, and F. Giordano, Active deformation and volcanism offshore Campi Flegrei, Itlay: New data from high-resolution seismic reflection profiles, *Mar. Geol.*, **171**, 61–73, 2000.

Morgan, L. A., Geophysical characteristics of volcanogenic massive sulfide deposits, in *Volcanogenic Massive Sulfide Occurrence Model*, edited by W. C. P. Shanks III and R. Thurson, U.S. Geological Survey Scientific Investigations Report 2010-5070-C, 117–131, U.S.A., 2002.

Morgan, L. A., Geophysical characteristics of volcanogenic massive sulfide deposits, in *Volcanogenic Massive Sulfide Occurrence Model*, edited by W. C. P. Shanks III and R. Thurson, U.S. Geological Survey Scientific Investigations Report 2010-5070-C, 117–131, U.S.A., 2012.

Mueller, W. U., R. Daigheault, B. Lafrance, J. Stix, P. L. Corcoran, and V. Pearson, Abitibi subaqueous calderas with volcanogenic massive sulfide deposits: Exploration models and hydrothermal carbonate alteration, in *Submarine Volcanism and Mineralization: Modern Through Ancient*, edited by B. Cousens and S. J. Piercey, Geological Association of Canada, Short Course Notes 19, 61–90, 2009.

Parker, R. L. and S. P. Huestis, The inversion of magnetic anomalies in the presence of topography, *J. Geophys. Res.*, **79**, 1587–1593, 1974.

Pelletier, B., S. Calmant, and R. Pillet, Current tectonics of the Tonga-New Hebrides region, *Earth Planet. Sci. Lett.*, **164**, 263–276, 1998.

Roche, O., T. H. Druitt, and O. Merle, Experimental study of caldera formation, *J. Geophys. Res.*, **105**, 395–416, 2000.

Schwarz-Schampera, U., R. Botz, M. Hannington, R. Adamson, V. Anger, D. Cormany, L. Evans, H. Gibson, K. Haase, W. Hirdes, M. Hocking, K. Juniper, S. Langley, M. Leybourne, A. Metaxas, R. Mills, Chr. Ostertag-Henning, M. Rauch, J. Rutkowski, M. Schmidt, K. Shepherd, C. Stevens, K. Tamburri, D. Tracey, and U. Westrnstroer, Cruise Report SONNE 192/2 MANGO, 92 pp., 2007.

Stix, J., B. Kennedy, M. Hannington, H. Gibson, R. Fiske, W. Mueller, and J. Franklin, Caldera-forming processes and the origin of submarine volcanogenic massive sulfide deposits, *Geology*, **31**, 375–378, 2003.

Stoffers, P., T. J. Worthington, U. Schwarz-Schampera, M. D. Hannington, G. J. Massoth, R. Hekinian, M. Schmidt, L. J. Lundsten, L. J. Evans, R. Vaiomo'unga, and T. Kerby, Submarine volcanoes and high-temperature hydrothermal venting on the Tonga arc, southwest Pacific, *Geology*, **34**, 453–456, 2006.

H.-J. Kim (e-mail: hanjkim@kiost.ac), H.-T. Jou, G.-H. Lee, J.-H. Na, H.-S. Kim, U. Jang, K.-Y. Lee, C.-H. Kim, S. H. Lee, C.-H. Park, S.-K. Jung, and B.-C. Suk